Egypt. J. Chem. **Vol. 67,** No. 4 pp. 251 - 271 (2024)

Egyptian Journal of Chemistry

http://ejchem.journals.ekb.eg/

Electro-osmotic peristaltic flow of non-Newtonian nanofluid Al_2O_3 inside a microchannel with modified Darcy's law and activation energy

N. T. Eldabe,[a] M. Y. Abouzeid,[a] M. M. Abdelmoneim [*,a] and M. E. Ouaf [a]

[a]*Department of Mathematics, Faculty of Education, Ain Shams University, Cairo, Egypt*

Abstract

The main objective of this study was to investigate the peristaltic flow of an unsteady non-Newtonian nanofluid through a uniformly symmetric vertical duct. The investigation was conducted considering the presence of external electric and magnetic fields, which led to the occurrence of both electroosmosis and induced magnetic field phenomena. The non-Newtonian fluid obeys the third-order model. Furthermore, the flow is through a porous medium which follows the modified form of Darcy's law. The study also considered the influences of mixed convection, Dufour and Soret, chemical reaction, activation energy, viscous dissipation, and heat generation in the system. To simplify the governing equations that describe velocity, temperature, and nanoparticle concentration, wave transformation techniques were employed. The resulting simplified equations were then analytically solved using the homotopy perturbation method (HPM). Furthermore, a set of figures were utilized to visually illustrate and discuss the influence of the various physical parameters involved in the problem on the solutions obtained. The investigation provided a clearer understanding of the relationships and effects of the parameters on the system's behavior. It is found that the modified Darcy term significantly extends the impact of permeability in the porous medium (near the walls) to the core flow (middle of the tube). As a result, the axial velocity is enhanced in the flow direction. Moreover, the investigation reveals a clear correlation between the permeability parameter and the electro-osmotic parameter. This relationship exists due to the inverse proportionality between the electro-osmotic parameter and the length of the electric double layer (EDL) that is formed adjacent to the walls of the tube (high porous region). Furthermore, it is found that as the activation energy increases the rate of the chemical reaction is reduced which in turn reduces the concentration of nanoparticles. Additionally, it is found that as the external magnetic field strength increases the nanoparticles are more concentrated which helps in many biological applications such as drug delivery. Conversely, as induced electric field strength increases the nanoparticles disperse through the fluid.

Keywords: peristaltic flow, electro-osmotic flow, non-Newtonian fluid, nanofluid, activation energy**,** modified Darcy's law**,** induced magnetic field.

1. Introduction

Nanofluids are a new class of fluid formulated by dispersing nanoparticles, which are particles with dimensions less than 100 nanometers, into a base fluid such as water, oil, or ethylene glycol. These nanoparticles are typically made from metals, oxides, carbides, or carbon nanotubes. The addition of these nanoparticles can significantly enhance the thermal, electrical, and magnetic properties of the base fluid, making nanofluids highly useful in various applications including cooling systems for electronics, vehicles, and nuclear reactors, as well as in solar energy and heat exchanger systems. Nonetheless, the utilization of nanofluids is not without challenges. In addition to the elevated costs associated with production, there is a problem with nanoparticle agglomeration over time. This aggregation can cause blockages and reduce the effectiveness of heat transfer in the nanofluid. Furthermore, as the nanoparticles cluster, they contribute to an increase in both the viscosity and density of the fluid. This increase can lead to a more significant pressure drop in the system and require additional pumping power [1]. Consequently, numerous researchers have expressed interest in investigating the flow of nanofluids under different

*Corresponding author e-mail: supermaged93@gmail.com (M. Abdelmoneim)
Receive Date: 14 September 2023, Revise Date: 18 October 2023, Accept Date: 25 October 2023
DOI: https://doi.org/10.21608/ejchem.2023.236533.8619

external influences. Hussein and Eldabe [2] studied the peristaltic motion of a nanofluid, which followed Carreau's model, through a vertical irregular duct, in their study several factors are considered such as induced magnetic field, viscous dissipation, and mixed convection. Eldabe et al. [3] investigated the peristaltic flow of a magnetohydrodynamic (MHD) Herschel Bulkley nanofluid within a non-uniform vertical channel. The flow occurred through a non-Darcy porous medium, and the study also took into account the influences of Ohmic dissipation, thermal radiation, chemical reaction, and slip boundary conditions. Abuiyada et al. [4] focused on MHD peristaltic flow of Jeffery nanofluid through a porous media. The study took into account the effects of several factors such as thermal radiation, Ohmic dissipation, and the presence of a non-Darcy porous medium. Mohamed et al. [5] examined the flow of Eyring-Powell nanofluid through a Darcy porous medium, the impact of several factors such as Cattaneo-Christov, double diffusion, and thermal radiation were considered. Eldabe et al. [6] conducted research on MHD peristaltic flow involving Bingham nanofluid within a symmetric uniform channel with specific wall properties. Their investigation explored various factors, including Brownian motion, thermophoresis, Joule heating, and chemical reactions. Eldabe et al. [7] investigated the effects of Cattaneo-Christov heat flux, Soret and Dufour diffusion, and Hall current on the peristaltic flow of a micropolar non-Newtonian nanofluid within a tapered stenosed artery. The study employed the tangent hyperbolic model to describe the fluid behavior and considered additional factors, such as heat generation/absorption, Joule heating, thermal radiation, chemical reactions, and the permeability of the porous medium. Ouaf et al. [8] conducted a study that examined the influence of entropy generation and slip velocity conditions on the flow MHD Jeffery nanofluid flow through a porous medium within a peristaltic channel. Their investigation also accounted for the effects of mixed convection, heat sources, double diffusion, and chemical reactions. Eldabe et al. [9] studied the peristaltic transport of Jeffry nanofluid within a vertical duct, taking into consideration various external influences, including a porous medium, a uniform magnetic field, viscous dissipation, internal heat generation, and thermal radiation. The cited references [10–17] encompass recent studies that have concentrated on investigating the peristaltic flow of nanofluids under diverse external influences.

Non-Newtonian fluids, such as polymer solutions, blood, mucus, ketchup, toothpaste, etc., exhibit complex rheology (deformation) characterized by the nonlinear correlation between its strain and the applied shear stress. These fluids can be classified into several categories based on their unique behaviors, such as shear-thinning (Pseudoplastic), shear-thickening (Dilatant), viscoelastic, and viscoplastic fluids. Given this complexity, relying on a single model is inadequate for their accurate representation. Consequently, multiple models are employed to investigate the flow behavior of these fluids. In recent years, the utilization of non-Newtonian fluids has witnessed a remarkable surge across diverse industries, such as chemical, petrochemical, food processing, metallurgy, drilling, and bioengineering. Extensive research has been carried out to gain a deeper understanding of the flow behavior of different types of non-Newtonian fluids under various external influences. Eldabe et al. [18] investigated the peristaltic flow of Bingham blood fluid in a non-uniform channel, considering heat and mass transfer, along with the influence of several external factors. These factors include a uniform magnetic field, thermal diffusion, diffusion thermo effects, as well as ohmic and viscous dissipation. Additionally, the study accounted for chemical reactions. Eldabe et al. [19] conducted a research on the MHD flow of third-grade nanofluid through a porous medium within the gap between two coaxial tubes. The inner tube was rigid, while the outer tube featured a sinusoidal wave propagating along its wall. The study considered the influence of heat sources and chemical reactions. Eldabe et al. [20] conducted research on the peristaltic motion of Bingham nanofluid through a non-Darcy porous medium. They investigated the flow under the effects of various factors, including thermal diffusion, heat generation, chemical reaction, and mixed convection. Akbar et al. [21] studied the MHD peristaltic flow Powell-Eyring nanofluid, taking into account the presence of the electroosmosis phenomenon and a porous medium. In addition, the study investigated the behavior of the flow considering variable thermal conductivity, chemical reactions, and mixed convection. Eldabe et al. [22] conducted a study on the peristaltic transport of Casson fluid through a porous medium inside a horizontal annulus. The investigation took into account various external effects, including Hall current, radiation, thermo-diffusion, diffusion-thermo effects, and chemical reaction.

Magneto-hydrodynamics (MHD) focuses on investigating the dynamics of electrically conductive fluids when subjected to a magnetic field. The fundamental equations governing MHD are based on Maxwell's equations. When a particle is in motion with velocity u and possesses a charge q, it experiences three electromagnetic forces. The first force is known as the electrostatic force (Coulomb force). It emerges from the interaction between electric charges, resulting in either repulsion or

attraction. The second force is the Lorentz force, which arises when the charged particle moves through a magnetic field. Lastly, the third force is the electromotive force (emf) and it arises due to the induced electric field caused by a varying magnetic field. However, the emf may be neglected at small magnetic Reynolds number. The magnetic Reynolds number (Rm) is the ratio of the induced magnetic field to the applied magnetic field. The low-Rm approximation holds true in three specific scenarios: (i) when the fluid moves slowly ensuring that the applied magnetic field remains constant without any changes. (ii) The applied magnetic field moves or rotates at a constant or slow rate. (iii) The applied magnetic field changes very fast such that the magnetic field stays near the surface of the fluid and does not penetrate inside. Categories (i) to (iii) encompass the majority of flow situations encountered in engineering applications such as the magnetic damping of jets, magnetic stirring, and magnetic levitation [23]. There are several studies that deal with the MHD peristaltic flow of non-Newtonian fluid under the assumption of low magnetic Reynolds number as cited in [24-28]. Conversely, the presence of an electromagnetic field (EMF) gives rise to a wide range of applications such as several types of electromagnetic flow meters, Electromagnetic blood flow measurement, and Electromagnetic water treatment. Eldabe et al. [30] conducted a pioneering study that examined the MHD peristaltic flow of biviscosity fluid flow under the influence of an induced magnetic field. Hayat et al. [31] initially investigated the peristaltic flow of a third-order fluid. They further extended their research in a subsequent study, by Hayat et al. [32], to analyze the impact of the induced magnetic field on the system. Ishtiaq et al. [33] investigated the flow of Jeffrey fluid with cilia movement, considering various factors including induced magnetic field and thermal radiation effects. References [34-36] provide additional studies that incorporate the analysis of induced magnetic fields.

In the presence of an external electric field, the surface in contact with the electrolyte solutions undergoes polarization, leading to the development of a charge (mainly negative). The charged surface attracts ions of opposite charge (counter-ions) and repels ions of similar charge (co-ions) within the solution. Consequently, a thin layer of fluid forms at the interface between the solid and liquid, known as the electric double layer (EDL). The EDL carries a net charge that balances the adjacent surface charge. Meanwhile, the bulk fluid outside of this layer remains electrically neutral, with an equal number of counter-ions and co-ions, resulting in a net charge density of zero throughout the region. The EDL comprises two primary components (as shown in Figure (2) [37]): the compact layer and the diffuse layer. The compact layer consists of counter-ions that exhibit strong affinity towards the surface, rendering them immobile. The compact layer is extremely thin, typically just a few Angstroms in thickness. Within this layer, the distribution of electric potential is primarily linear, meaning it decreases steadily across the compact layer. On the other hand, the diffuse layer is composed of counter-ions and co-ions. Co-ions share the same charge as the surface and are less strongly attracted, allowing them to move more freely within the solution. The boundary between the diffuse and compact layers is called the shear plane, where the electric potential known as the zeta potential exists. The zeta potential is commonly used as an approximation of the electric potential in the electrical double layer (EDL). When an electric field is applied, the mobile ions flow in the solution, causing fluid to be dragged along in a phenomenon called electro-osmotic flow (EOF). At the characteristic length scales of microfluidics, viscous forces outweigh inertial forces, resulting in bulk fluid motion outside the EDL. In 2006, Chakraborty [38] pioneered the development of a mathematical model to study the impact of electro-osmosis on peristaltic transport. This research mentioned that the major obstacle faced in the design of microfluidic transport systems lies in enhancing the rate of fluid flow utmost potential limit. It is found that the electro-osmosis phenomenon successfully achieves the desired speed of fluid movement through the designed microfluidic devices. Afterward, researchers became interested in investigating fluid flow under the influence of the electroosmotic effect. Abdelmoneim et al. [39] employed the homotopy perturbation method (HPM) to tackle the governing equations of peristaltic flow concerning a Papanastasiou non-Newtonian nanofluid. Their investigation encompassed the presence of a modified Darcy's porous medium, electro-osmosis phenomenon, mixed convection, chemical reaction, and viscous couple stress dissipation. Ramesh et al. [40] investigated the propulsion flow of MHD Sutterby nanofluid through a porous medium inside a microchannel. They considered various factors, including, electroosmosis, Hall currents, thermo-diffusion, and diffusion-thermo. Das and Barman [41] studied the peristaltic flow of a hybrid nanofluid in the presence of the electro-osmosis phenomenon and Darcy's porous medium. Additionally, they examined the influences of Hall and ion-slip currents.

The present paper focuses on studying the behavior of a non-Newtonian nanofluid, specifically following the third-order model, within a vertical channel subjected to peristaltic motion along the walls. Furthermore, the analysis incorporates the impact of external electric and magnetic fields, resulting in the phenomena of electro-osmosis and induced magnetic field. Moreover, the fluid flow

occurs through a porous medium, adhering to a modified formulation of Darcy's law. In this modification, the apparent viscosity of the fluid, rather than the Newtonian viscosity, is considered within the porous term. Additionally, the study takes into consideration the impact of several other factors such as mixed convection, heat generation, and chemical reactions with activation energy.

2. Mathematical formulation of the problem

We investigated the flow of an incompressible non-Newtonian nanofluid inside a symmetric channel with peristalsis. The non-Newtonian fluid obeys the third-grade model and the porous medium follows a modified Darcy model. Additionally, we are taking into account various factors such as electro-osmotic phenomena, induced magnetic field, and chemical reactions involving activation energy. In Figure 1, Cartesian coordinates (X, Y) are chosen to represent the system. The X-axis corresponds to the symmetric axis of the micro-channel, while the Y-axis is perpendicular to it. The walls of the channel are depicted by dotted lines, while the peristaltic movement is indicated by solid lines. The temperature and concentration at the left wall are denoted by $T_\bullet$ and $C_\bullet$, respectively, while $T_\bullet$ and $C_\bullet$ are the temperature and the concentration at the right wall. The wall equations for symmetric channel can be written as:

$$Y = \pm\left(h + a\,Cos\left(\frac{\pi}{\lambda}(X - ct) \right) \right). \tag{1}$$

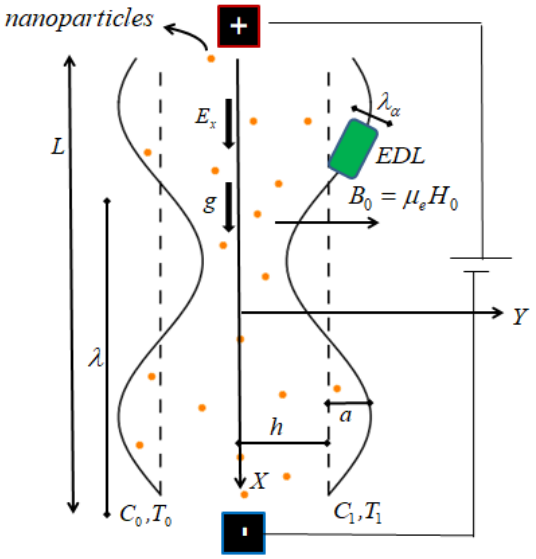

Figure 1: Physical model and coordinates system

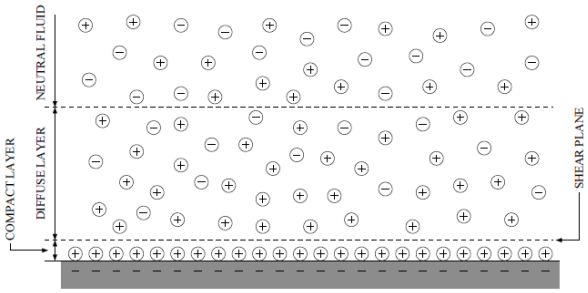

Figure 2: Diagram of the electric double layer (EDL)

In the laboratory frame (X, Y), the vector form of the governing equations can be written as:

$$\nabla . \vec{V} = \bullet\ , \tag{2}$$

$$\rho_f \left(\frac{\partial}{\partial t} + \vec{V}.\nabla \right) \vec{V} = -\nabla P + \nabla . \vec{\tau} + \rho_f \vec{g} \begin{pmatrix} \beta_t (T - T_\bullet) \\ + \beta_c (T - T_\bullet) \end{pmatrix} + \vec{R} + \vec{F}_m + \vec{F}_e , \tag{3}$$

$$(\rho c)_f \left(\frac{\partial}{\partial t} + \vec{V}.\nabla \right) T = K_c \nabla^{\bullet} T + \vec{\tau}. \nabla \vec{V} + (\rho c)_p \begin{pmatrix} D_B (\nabla T \nabla C) \\ + \frac{D_T}{T_m} (\nabla^{\bullet} T) \end{pmatrix} + Q_\bullet (T - T_\bullet) + \xi \vec{F}_e^{\bullet} , \tag{4}$$

$$\left(\frac{\partial}{\partial t} + \vec{V}.\nabla \right) C = D_B (\nabla^{\bullet} C) + \frac{D_T}{T_m} (\nabla^{\bullet} T) - A \left(\frac{T}{T_\bullet} \right)^n Exp\left[\frac{-E_a}{K_B T} \right] (C - C_\bullet) , \tag{5}$$

where,

$$\left. \begin{aligned} \vec{V} &= (U(X,Y,t),\ V(X,Y,t)), \\ \vec{g} &= (g, \bullet), \\ \vec{F}_e &= \rho_e (E_x, \bullet) \end{aligned} \right\}, \tag{6}$$

Maxwell's equation states that [23]:

$$\nabla \cdot \vec{E} = \frac{\rho_e}{\varepsilon} , \tag{7(a)}$$

$$\nabla \cdot \vec{B}^+ = \bullet\ , \tag{7(b)}$$

$$\nabla \times \vec{E} = -\frac{\partial \vec{B}^+}{\partial t} , \tag{7(c)}$$

$$\vec{J} = \frac{\bullet}{\mu_e} \nabla \times \vec{B}^+ - \varepsilon_\bullet \frac{\partial \vec{E}}{\partial t} , \tag{7(d)}$$

where,

$$\vec{J} = \varepsilon_{\bullet}\left(\vec{E} + \vec{V} \times \vec{B}^{+}\right). \tag{8}$$

The Lorentz force $\vec{F}_m$ is defined as

$$\vec{F}_m = \vec{J} \times \vec{B}^{+} . \tag{9}$$

In the free space, the external magnetic field $\vec{B}$ is defined as:

$$\vec{B} = \mu_e \vec{H} = \mu_e\left(\bullet, H_{\bullet}\right), \tag{10}$$

the induced magnetic field $\vec{B}_I$ is defined as:

$$\vec{B}_I = \mu_e \vec{H}_I = \mu_e\left(h_x(X,Y,t), h_y(X,Y,t)\right), \tag{11}$$

the total magnetic field $\vec{B}^{+}$ is defined as [35]:

$$\left.\begin{aligned} \vec{B}^{+} &= \vec{B} + \vec{B}_I \\ &= \mu_e \vec{H}^{+} \\ &= \mu_e\left(h_x, H_{\bullet} + h_y\right) \end{aligned}\right\}. \tag{12}$$

considering $\frac{\partial \vec{E}}{\partial t} = \bullet$ and applying the following vector identities:

$$\left.\begin{aligned} \left(\nabla \times \vec{B}^{+}\right)\vec{B}^{+} &= \left(\vec{B}^{+}.\nabla\right)\vec{B}^{+} - \left(\nabla \vec{B}\right).\vec{B}^{+}, \\ \left(\nabla \vec{B}\right).\vec{B}^{+} &= \frac{\bullet}{\bullet}\nabla^{\bullet}\vec{B}^{+} \end{aligned}\right\} \tag{13}$$

hence, Eq. (9) be written as :

$$\vec{F}_m = \mu_e\left(\left(\vec{H}^{+}.\nabla\right)\vec{H}^{+} - \frac{\bullet}{\bullet}\nabla^{\bullet}\vec{H}^{+}\right). \tag{14}$$

Considering $\frac{\partial \vec{E}}{\partial t} = \bullet$ and using the Eqs. 7(d), (8) and (12) then the induced magnetic equation is formed as follows:

$$\vec{E} = \frac{\bullet}{\varepsilon_{\bullet}}\nabla \times \vec{H}^{+} - \mu_e \vec{V} \times \vec{H}^{+}, \tag{15}$$

this implies that $\vec{E} = \left(0,0,E_z\right)$ such that:

$$\left.\begin{aligned} E_z = \frac{\bullet}{\varepsilon_{\bullet}}\left(\frac{\partial\left(H_{\bullet} + h_y\right)}{\partial x} - \frac{\partial h_x}{\partial y}\right), \\ - \mu_e\left(U\left(H_{\bullet} + h_y\right) - V\right) \end{aligned}\right. \tag{16}$$

Considering the external electric field can be treated as a conservative field, this means that it can be expressed as the gradient of a scalar potential function, known as the electric potential. Then the wall zeta potential ϕ may be described by the Poisson-Boltzmann equation as follows:

$$\rho_e = -\varepsilon_{\bullet}\,\nabla^{\bullet}\phi, \tag{17}$$

In the context of a symmetric binary electrolyte solution, assuming the same concentration of positive and negative ions,

$$\rho_e = e\,z\left(n^{+} - n^{-}\right), \tag{18}$$

where,

$$n^{\pm} = N_{\bullet}\,Exp\left[\mp\frac{e\,z\phi}{k_B T_{av}}\right], \tag{19}$$

Using equation (19) in (18), then substitute in equation (17), thus:

$$\nabla^{\bullet}\phi = \frac{\bullet\, N_{\bullet}\, e\, z}{\varepsilon_{\bullet}}\,Sinh\left[\frac{e\,z}{k_B T_{av}}\phi\right]. \tag{20}$$

Considering the value of ϕ is small enough to apply the Debye-Huckel linearization approximation, the equation can be simplified as follows:

$$\nabla^{\bullet}\phi = \frac{\bullet\, N_{\bullet}\, e^{\bullet} z^{\bullet}}{\varepsilon_{\bullet}\, k_B T_{av}}\phi . \tag{21}$$

The extra stress tensor ($\vec{\tau}$) for the third order fluid is given by:

$$\begin{aligned} \vec{\tau} = {} & \mu_0 \vec{A}_{\bullet} + \alpha_1 \vec{A}_{\bullet} + \alpha_2 \vec{A}_{\bullet}^{\bullet} \\ & + \beta_1 \vec{A}_{\bullet} + \beta_2\left(\vec{A}_{\bullet}.\vec{A}_{\bullet} + \vec{A}_{\bullet}.\vec{A}_{\bullet}\right), \\ & + \beta_3\left(\left(tr\vec{A}_{\bullet}^{\bullet}\right)\vec{A}_{\bullet}\right) \end{aligned} \tag{22}$$

Where

$$\left.\begin{aligned} \nabla \vec{V} &= \begin{pmatrix} \partial U/\partial X & \partial U/\partial Y \\ \partial V/\partial X & \partial V/\partial Y \end{pmatrix}, \\ \left(\nabla \vec{V}\right)^{T} &= \begin{pmatrix} \partial U/\partial X & \partial V/\partial X \\ \partial U/\partial Y & \partial V/\partial Y \end{pmatrix} \end{aligned}\right\}, \tag{23}$$

$$\left.\begin{aligned} \vec{A}_{\bullet} &= \nabla \vec{V} + \left(\nabla \vec{V}\right)^{T}, \\ \vec{A}_n &= \left(\frac{\partial}{\partial t} + \vec{V}\,\nabla\right)\vec{A}_{n-\bullet} \\ &\quad + \vec{A}_{n-\bullet}\nabla \vec{V} + \left(\nabla \vec{V}\right)^{T}\vec{A}_{n-\bullet}, \quad n > 1 \end{aligned}\right\}, \tag{24}$$

Considering the following conditions:

$$\left.\begin{aligned} &\mu_{\bullet} \geq \bullet\ , \\ &\beta_{\bullet} \geq \bullet, \\ &\left|\alpha_{\bullet} + \alpha_{\bullet}\right| \geq \sqrt{\bullet \bullet \mu_{\bullet}.\beta_{\bullet}}\ , \\ &\beta_{\bullet} = \beta_{\bullet} = \bullet \end{aligned}\right\}, \tag{25}$$

the flow of the fluid conforms to the Clausius-Duhem inequality. Additionally, at equilibrium, the fluid's specific Helmholtz free energy attains its minimum value. Hence, Eq. (22) is reduced to [42],

$$\vec{\tau} = \left(\mu_0 + \beta_3\left(tr\vec{A}_{\bullet}^{\bullet}\right)\right)\vec{A}_{\bullet} + \alpha_1 \vec{A}_{\bullet} + \alpha_2 \vec{A}_{\bullet}^{\bullet} . \tag{26}$$

Using Eq. (2) and Eqs. (23, 24) in (26), hence:

$$\vec{\tau} = \begin{pmatrix} \tau_{xx} & \tau_{yx} \\ \tau_{xy} & \tau_{yy} \end{pmatrix}, \text{ where}$$

$$\tau_{xx} = \bullet \begin{pmatrix} \mu_{\bullet} + \bullet \beta_{\bullet} \left(\frac{\partial U}{\partial Y} + \frac{\partial V}{\partial X} \right)^{\bullet} \\ - \bullet \beta_{\bullet} \frac{\partial U}{\partial X} \frac{\partial V}{\partial y} \end{pmatrix} \frac{\partial U}{\partial X}$$
$$+ \bullet \alpha_{\bullet} \begin{pmatrix} \frac{\partial^{\bullet} U}{\partial X \partial t} + U \frac{\partial^{\bullet} U}{\partial X^{\bullet}} + V \frac{\partial^{\bullet} U}{\partial X \partial Y} \\ + \bullet \left(\frac{\partial U}{\partial X} \right)^{\bullet} + \frac{\partial V}{\partial X} \left(\frac{\partial U}{\partial Y} + \frac{\partial V}{\partial X} \right) \end{pmatrix}, \quad (27)$$
$$+ \alpha_{\bullet} \left(\bullet \left(\frac{\partial U}{\partial X} \right)^{\bullet} + \left(\frac{\partial U}{\partial Y} + \frac{\partial V}{\partial X} \right)^{\bullet} \right)$$

$$\tau_{xy} = \tau_{yx}$$
$$= \begin{pmatrix} \mu_{\bullet} \\ + \bullet \beta_{\bullet} \left(\frac{\partial U}{\partial Y} + \frac{\partial V}{\partial X} \right)^{\bullet} \\ - \bullet \beta_{\bullet} \frac{\partial U}{\partial X} \frac{\partial V}{\partial Y} \end{pmatrix} \left(\frac{\partial U}{\partial Y} + \frac{\partial V}{\partial X} \right)$$
$$+ \bullet \alpha_{\bullet} \begin{pmatrix} \frac{\partial^{\bullet} U}{\partial Y \partial t} + \frac{\partial^{\bullet} V}{\partial X \partial t} + U \frac{\partial^{\bullet} U}{\partial X \partial Y} \\ + V \frac{\partial^{\bullet} V}{\partial X \partial Y} + U \frac{\partial^{\bullet} V}{\partial X^{\bullet}} \\ + V \frac{\partial^{\bullet} U}{\partial Y^{\bullet}} + \bullet \left(\frac{\partial U}{\partial X} \frac{\partial U}{\partial Y} \right) \\ + \bullet \left(\frac{\partial V}{\partial X} \frac{\partial V}{\partial Y} \right) \end{pmatrix}, \quad (28)$$

$$\tau_{yy} = \bullet \begin{pmatrix} \mu_0 + \bullet \beta_3 \left(\frac{\partial U}{\partial Y} + \frac{\partial V}{\partial X} \right)^{\bullet} \\ - \bullet \beta_3 \frac{\partial U}{\partial X} \frac{\partial V}{\partial y} \end{pmatrix} \frac{\partial V}{\partial Y}$$
$$+ \bullet \alpha_1 \begin{pmatrix} \frac{\partial^{\bullet} V}{\partial Y \partial t} + \bullet U \frac{\partial^{\bullet} V}{\partial X \partial Y} \\ + \bullet V \frac{\partial^{\bullet} V}{\partial Y^{\bullet}} + \bullet \left(\frac{\partial V}{\partial Y} \right)^{\bullet} \\ + \bullet \left(\frac{\partial U}{\partial Y} \right)^{\bullet} + \bullet \frac{\partial U}{\partial Y} \frac{\partial V}{\partial X} \end{pmatrix} \quad . \quad (29)$$
$$+ \alpha_2 \left(\bullet \left(\frac{\partial V}{\partial Y} \right)^{\bullet} + \left(\frac{\partial U}{\partial Y} + \frac{\partial V}{\partial X} \right)^{\bullet} \right)$$

The modified Darcy's term $\vec{R}$ is defined as

$$\vec{R} = - \frac{\mu\left(\left| \vec{A}_{\bullet} \right| \right)}{k} \vec{V} \ . \quad (30)$$

where,

$$\mu\left(\left| \vec{A}_{\bullet} \right| \right) = \left(\mu_0 + \beta_3 \left(tr \vec{A}_{\bullet}^{\bullet} \right) \right)$$
$$= \begin{pmatrix} \mu_0 + \bullet \beta_3 \left(\frac{\partial U}{\partial Y} + \frac{\partial V}{\partial X} \right)^{\bullet} \\ - \bullet \beta_3 \frac{\partial U}{\partial X} \frac{\partial V}{\partial y} \end{pmatrix}. \quad (31)$$

Notice that, in the case of a Newtonian fluid $(\beta_3 = \bullet)$, the modified Darcy's term will be $\vec{R} = - \frac{\mu_{\bullet}}{k} \vec{V}$.

Taking into account the subsequent transformations:

$$\left. \begin{array}{l} x = X - \bar{c} t, \quad Y = y, \\ u(x,y) = U(X,Y,t) - \bar{c}, \\ v(x,y) = V(X,Y,t), \\ p(x,y) = P(X,Y,t) \end{array} \right\}, \quad (32)$$

where (x,y) are the coordinates in the moving frame and (u,v) are the velocity coordinates concerning this frame. The governing Eqs. (2–5) and (16) can be written as

$$\frac{\partial u}{\partial x} + \frac{\partial v}{\partial y} = \bullet , \quad (33)$$

$$\rho_f \left(u \frac{\partial u}{\partial x} + v \frac{\partial u}{\partial y} \right) = \frac{- \partial p}{\partial x} + \frac{\partial \tau_{xx}}{\partial x} + \frac{\partial \tau_{xy}}{\partial y}$$
$$+ \rho_f \, g \begin{bmatrix} \beta_t (T - T_{\bullet}) \\ + \beta_c (f - f_{\bullet}) \end{bmatrix}$$
$$+ \mu_e \begin{pmatrix} h_x \frac{\partial h_x}{\partial x} + (h_y + H_{\bullet}) \frac{\partial h_x}{\partial y} \\ - \frac{\bullet}{\bullet} \frac{\partial^{\bullet} h_x}{\partial x^{\bullet}} \end{pmatrix}, \quad (34)$$
$$- \varepsilon \left(\frac{\partial^{\bullet} \phi}{\partial x^{\bullet}} + \frac{\partial^{\bullet} \phi}{\partial y^{\bullet}} \right) E_x + R_x$$

$$\rho_f \left(u \frac{\partial v}{\partial x} + v \frac{\partial v}{\partial y} \right) = \frac{- \partial p}{\partial y} + \frac{\partial \tau_{yx}}{\partial x} + \frac{\partial \tau_{yy}}{\partial y}$$
$$+ \mu_e \begin{pmatrix} h_x \frac{\partial h_y}{\partial x} + (h_y + H_{\bullet}) \frac{\partial h_y}{\partial y} \\ - \frac{\bullet}{\bullet} \frac{\partial^{\bullet} h_y}{\partial y^{\bullet}} \end{pmatrix} + R_y \quad , \quad (35)$$

$$(\rho c)_f\left(u\frac{\partial T}{\partial x}+v\frac{\partial T}{\partial y}\right)=K_c\left(\frac{\partial^{\cdot} T}{\partial x^{\cdot}}+\frac{\partial^{\cdot} T}{\partial y^{\cdot}}\right)+\tau_{xx}\frac{\partial u}{\partial x}+\tau_{yy}\frac{\partial v}{\partial y}+\tau_{xy}\left(\frac{\partial u}{\partial y}+\frac{\partial v}{\partial x}\right)+(\rho c)_p\left\{\begin{array}{l}D_B\left(\frac{\partial T}{\partial x}\frac{\partial C}{\partial x}+\frac{\partial T}{\partial y}\frac{\partial C}{\partial y}\right)\\+\frac{D_T}{T_m}\left[\left(\frac{\partial T}{\partial x}\right)^2+\left(\frac{\partial T}{\partial y}\right)^2\right]\end{array}\right\}+\sigma E_x^{\cdot}+Q_0\left(T-T_0\right) \quad (36)$$

$$u\frac{\partial C}{\partial x}+v\frac{\partial C}{\partial y}=D_B\left(\frac{\partial^{\cdot} C}{\partial x^{\cdot}}+\frac{\partial^{\cdot} C}{\partial y^{\cdot}}\right)+\frac{D_T}{T_m}\left(\frac{\partial^{\cdot} T}{\partial x^{\cdot}}+\frac{\partial^{\cdot} T}{\partial y^{\cdot}}\right)-A\left(\frac{T}{T_{\cdot}}\right)^n Exp\left[\frac{-E_a}{K_B T}\right]\left(C-C_{\cdot}\right) \quad (37)$$

Where,

$$R_x=-\frac{\cdot}{k}\left(\begin{array}{l}\mu_0+\cdot\beta_3\left(\frac{\partial U}{\partial Y}+\frac{\partial V}{\partial X}\right)^{\cdot}\\-\cdot\beta_3\frac{\partial U}{\partial X}\frac{\partial V}{\partial y}\end{array}\right)\left(u+\bar{c}\right), \quad (38)$$

$$R_y=-\frac{\cdot}{k}\left(\begin{array}{l}\mu_0+\cdot\beta_3\left(\frac{\partial U}{\partial Y}+\frac{\partial V}{\partial X}\right)^{\cdot}\\-\cdot\beta_3\frac{\partial U}{\partial X}\frac{\partial V}{\partial y}\end{array}\right)v, \quad (39)$$

The boundary conditions that are relevant to the governing equations and the wall zeta ϕ potential in the moving frame can be expressed as:

$$\left.\begin{array}{l}at\ \ y=-H=-h-aSin\left(\frac{\cdot\pi}{\lambda}x\right):\\T=T_0,\ C=C_0,\quad u=-\bar{c},\\at\ \ y=H=h+aSin\left(\frac{\cdot\pi}{\lambda}x\right):\\T=T_1,\ C=C_1,\quad u=-\bar{c},\ \phi=\zeta\\at\ \ y=\cdot:\\\frac{\partial\phi}{\partial y}=0,\end{array}\right\}, \quad (40)$$

Introducing the following dimensionless quantities:

$$\left.\begin{array}{l}\bar{x}=\frac{x}{\lambda},\ \bar{y}=\frac{y}{h},\ \bar{u}=\frac{u}{\bar{c}},\ \bar{v}=\frac{v}{\bar{c}\delta},\ \omega=\frac{a}{h},\\\delta=\frac{h}{\lambda},\ \bar{P}=\frac{h^2P}{\lambda\bar{c}\mu_0},\ \bar{H}=\frac{H}{h},\ \bar{k}=\frac{k}{h^2},\\N=\frac{\cdot\bar{c}^{\cdot}\beta_3}{h^{\cdot}\mu_0},\ G_r=\frac{h^2g\rho_f\beta_t\left(T_1-T_0\right)}{\bar{c}\mu_0},\\G_c=\frac{h^2g\rho_f\beta_c\left(f_1-f_{\cdot}\right)}{\bar{c}\mu_0},f=\frac{C-C_0}{C_1-C_0},\\\theta=\frac{T-T_0}{T_1-T_0},\ U_{HS}=-\frac{E_x\varepsilon_{\cdot}\zeta}{\mu_{\cdot}\bar{c}},\\\Omega=h\,z\,e\sqrt{\frac{2N_0}{\varepsilon_{\cdot}k_BT_{av}}}=\frac{h}{\lambda_\alpha},\ \bar{\phi}=\frac{\phi}{\zeta},\\h_x=\frac{\partial\xi}{\partial y},\ h_y=-\delta\frac{\partial\xi}{\partial x},\ \bar{\xi}=\frac{\xi}{H_0h},\\H_s=\frac{\mu_e hH_{\cdot}^{\cdot}}{\bar{c}\mu_0},\ R_m=\mu_e\varepsilon_{\cdot}h\bar{c},\\E=\frac{-E_z}{\mu_eH_{\cdot}\bar{c}},\ M^{\cdot}=H_sR_m,\\M=\mu_eH_{\cdot}h\sqrt{\frac{\varepsilon_{\cdot}}{\mu_0}},\ Re=\frac{\rho_f\bar{c}\,h}{\mu_0},\\Pr=\frac{\mu_{\cdot}c_f}{K_c},\ Ec=\frac{\bar{c}^{\cdot}}{c_f\left(T_1-T_0\right)},\\N_b\frac{(\rho c)_pD_B\left(c_1-c_{0.}\right)}{\mu_{\cdot}c_f},\\N_t=\frac{(\rho c)_pD_T\left(T_1-T_{0.}\right)}{\mu_{\cdot}c_fT_{av}},\\S=\frac{h^{\cdot}\sigma E_x^{\cdot}}{\mu_{\cdot}c_f\left(T_1-T_{0.}\right)},Q=\frac{h^{\cdot}Q_0}{\mu_{\cdot}c_f},\\\beta=\frac{T_1}{T_0},k_\alpha=\frac{Ah^2}{\nu_\mu},\ Sc=\frac{\nu_\mu}{D_B},\\E_A=\frac{E_a}{K_BT_{\cdot}},\ \tau_{xy}^{\ *}=\frac{h}{\bar{c}\mu_{\cdot}}\tau_{xy}\end{array}\right\} \quad (41)$$

Taking into account the low Reynolds number and long wavelength ($\delta\approx 0$), thereby, after dropping the bar mark, the dimensionless governing equations can be written as:

$$\frac{\partial p}{\partial x}=\frac{\partial^{\bullet} u}{\partial y^{2}}+\bullet N\left(\frac{\partial u}{\partial y}\right)^{\bullet}\frac{\partial^{\bullet} u}{\partial y^{2}}+G_c T+G_r f$$
$$+H_s\frac{\partial^{\bullet}\xi}{\partial y^{\bullet}}-\frac{\bullet}{k}(u+\bullet)-\frac{N}{k}\left(\frac{\partial u}{\partial y}\right)^{\bullet}(u+\bullet), \quad (42)$$
$$+U_{HS}\frac{\partial^{\bullet}\phi}{\partial y^{\bullet}}$$

Since, the dimensionless equation of Eq. (21) is:

$$\frac{\partial^{\bullet}\phi}{\partial y^{\bullet}}=\Omega^{\bullet}\ \phi. \quad (43)$$

Using the dimensionless boundary conditions in equation (40) the solution of equation (43) can be written as:

$$\phi=\frac{cosh(\Omega\, y)}{cosh(\Omega\, H)} \quad (44)$$

Hence, the Eq. (42) becomes:

$$\frac{\partial p}{\partial x}=\frac{\partial^{\bullet} u}{\partial y^{2}}+\bullet N\left(\frac{\partial u}{\partial y}\right)^{\bullet}\frac{\partial^{\bullet} u}{\partial y^{2}}+G_c T+G_r f$$
$$+H_s\frac{\partial^{\bullet}\xi}{\partial y^{\bullet}}-\frac{\bullet}{k}(u+\bullet)-\frac{N}{k}\left(\frac{\partial u}{\partial y}\right)^{\bullet}(u+\bullet), \quad (45)$$
$$+\Omega^{\bullet}\ U_{HS}\frac{cosh(\Omega\, y)}{cosh(\Omega\, H)}$$

using the dimensionless form of Eq. (16), hence [43]:

$$E=\frac{\bullet}{R_m}\left(\frac{\partial^{\bullet}\xi}{\partial y^{\bullet}}\right)+u+\bullet, \quad (46)$$

This equation indicates that in the case of low magnetic Reynolds number $(R_m\to\bullet)$, the effect of the induced magnetic function $\left(\frac{\partial^{\bullet}\xi}{\partial y^{\bullet}}=R_m(E-u-\bullet)\right)$ is neglected.

By utilizing Eq. (46), thus Eq. (45) is transformed into:

$$\frac{\partial p}{\partial x}=\frac{\partial^{\bullet} u}{\partial y^{2}}+\bullet N\left(\frac{\partial u}{\partial y}\right)^{\bullet}\frac{\partial^{\bullet} u}{\partial y^{2}}+G_c T+G_r f$$
$$+M^{\bullet}[E-u-\bullet]-\frac{\bullet}{k}(u+\bullet) \quad ,(47)$$
$$-\frac{N}{k}\left(\frac{\partial u}{\partial y}\right)^{\bullet}(u+\bullet)+\Omega^{\bullet}\ U_{HS}\frac{cosh(\Omega\, y)}{cosh(\Omega\, H)}$$

also,

$$\frac{\partial P}{\partial y}=\bullet, \quad (48)$$

$$\left(\frac{\partial^{\bullet}\theta}{\partial y^{\bullet}}\right)=-Pr\,Ec\left(\left(\frac{\partial u}{\partial y}\right)^{\bullet}+N\left(\frac{\partial u}{\partial y}\right)^{\bullet}\right)$$
$$-Pr\,N_b\left(\frac{\partial\theta}{\partial y}\frac{\partial f}{\partial y}\right)-Pr\,N_t\left(\frac{\partial\theta}{\partial y}\right)^{2} \quad , \quad (49)$$
$$-Pr\,S-Pr\,Q\,\theta$$

$$\frac{\partial^{\bullet} f}{\partial y^{\bullet}}+\frac{N_t}{N_b}\left(\frac{\partial^{\bullet}\theta}{\partial y^{\bullet}}\right)$$
$$=Sc\,k_{\alpha}(\bullet+(\beta-\bullet)\theta)^{n}\,Exp\left[-E_A(\bullet+(\beta-\bullet)\theta)^{-\bullet}\right]f \quad . \quad (50)$$

Given that $(\beta-\bullet)<<\bullet$ and utilizing the Taylor series expansion, Eq. (50) can be rewritten as:

$$\frac{\partial^{\bullet} f}{\partial y^{\bullet}}+\frac{N_t}{N_b}\left(\frac{\partial^{\bullet}\theta}{\partial y^{\bullet}}\right)$$
$$-Sc\,k_{\alpha}e^{-E_A}(\bullet+n(\beta-\bullet)\theta)(\bullet+E_A(\beta-\bullet)\theta)f=\bullet \quad . \quad (51)$$

Again using $(\beta-\bullet)<<\bullet$, then Eq. (51) becomes

$$\frac{\partial^{\bullet} f}{\partial y^{\bullet}}+\frac{N_t}{N_b}\left(\frac{\partial^{\bullet}\theta}{\partial y^{\bullet}}\right) \quad . \quad (52)$$
$$-Sck_{\alpha}e^{-E_A}(\bullet+(n+E_A)(\beta-\bullet)\theta)f=\bullet$$

The dimensionless boundary conditions correlated to the governing equations are:

$$\left.\begin{array}{l} at\ \ y=-H=-\bullet-\omega\,Sin(2\pi x): \\ u=-\bullet,\ \ \theta=0,\ \ f=\bullet, \\ at\ \ y=H=\bullet+\omega\ \ Sin(2\pi x): \\ u=-\bullet,\ \ \theta=1,\ \ f=\bullet,\ \ \phi=\bullet, \\ at\ \ y=\bullet\ : \\ \frac{\partial\phi}{\partial y}=0\ , \end{array}\right\}. \quad (53)$$

The reduced Nusselt number and the skin friction coefficient are of notable interest and are defined

$$\left.\begin{array}{l} Nu(x)=\left.\frac{\partial T}{\partial y}\right|_{y=H} \\ \tau_{\omega}(x)=\left.\tau_{xy}\right|_{y=H} \end{array}\right\} \quad (54)$$

The dimensionless form is:

$$\left.\begin{aligned} Nu(x) &= \left.\frac{\partial \theta}{\partial y}\right|_{y=H=\bullet+\omega\ Sin(2\pi x)} \\ \tau_{\omega}(x) &= \left[\frac{\partial u}{\partial y} + N\left(\frac{\partial u}{\partial y}\right)^{\cdot}\right]_{y=H=\bullet+\omega\ Sin(2\pi x)} \end{aligned}\right\} \tag{55}$$

3. Method of solution:

In order to solve the system of non-linear partial differential equations governed by equations (47), (49), and (52), along with the associated boundary conditions (53), the homotopy perturbation method (HPM) was employed.

Since $u \equiv u(x,y)$,where $f \equiv f(x,y), \theta \equiv \theta(x,y)$ therefore by $, y \equiv H(x) = \bullet + \omega\ Sin(2\pi x)$ considering a vertical slice of the channel (fix value of x), thereby $u \equiv u(y)$,and $f \equiv f(y), \theta \equiv \theta(y)$ the boundary conditions is taken at $y = \pm H = \bullet$.

As a result, the system of governing equations is treated as a set of ordinary differential equations (ODEs).

Considering $\omega_{\cdot}$ is a small parameter, such that $\bullet < \omega_{\cdot} \leq \bullet$ so that the system of the equations is written as:

$$\frac{\partial^{\cdot} u}{\partial y^{2}} = S_{\cdot} + \omega_{0}\left\{\begin{aligned} & S_{\cdot}u + S_{\cdot}\left(\frac{\partial u}{\partial y}\right)^{\cdot}\frac{\partial^{\cdot} u}{\partial y^{2}} \\ & + S_{\cdot}\theta + S_{\cdot}f + \\ & S_{\cdot}\left(\frac{\partial u}{\partial y}\right)^{\cdot}(u+\bullet) \\ & + S_{\cdot}\ cosh(\Omega\, y) \end{aligned}\right\}, \tag{56}$$

$$\frac{\partial^{\cdot} \theta}{\partial y^{2}} = B_{\cdot} + \omega_{0}\left\{\begin{aligned} & B_{\cdot}\theta + B_{\cdot}\left(\frac{\partial u}{\partial y}\right)^{\cdot} + \\ & B_{\cdot}\left(\frac{\partial u}{\partial y}\right)^{\cdot} \\ & + B_{\cdot}\left(\frac{\partial \theta}{\partial y}\right)\left(\frac{\partial f}{\partial y}\right) \\ & + B_{\cdot}\left(\frac{\partial \theta}{\partial y}\right)^{\cdot} \end{aligned}\right\}, \tag{57}$$

$$\frac{\partial^{\cdot} f}{\partial y^{\cdot}} = \omega_{0}\left\{E_{\cdot}\frac{\partial^{\cdot} \theta}{\partial y^{\cdot}} + E_{\cdot}f + E_{\cdot}f\theta\right\}, \tag{58}$$

where,

$$\left.\begin{aligned} u(y) &= u_{\cdot}(y) + \omega_{0}\ u_{\cdot}(y) + \omega_{0}^{\cdot}\ u_{\cdot}(y) + ... \\ \theta(y) &= \theta_{\cdot}(y) + \omega_{0}\ \theta_{\cdot}(y) + \omega_{0}^{\cdot}\ \theta_{\cdot}(y) + ... \\ f(y) &= f_{\cdot}(y) + \omega_{0}\ f_{\cdot}(y) + \omega_{0}^{\cdot}\ f_{\cdot}(y) \\ &\quad + \omega^{\cdot}\ f_{\cdot}(y) + ... \end{aligned}\right\}, \tag{59}$$

with the boundary conditions:

$$\left.\begin{aligned} & u_{\cdot} = -\bullet\ ,\ u_{\cdot} = u_{\cdot} = ... = \bullet \\ & \theta_{\cdot} = \theta_{\cdot} = \theta_{\cdot} = ... = \bullet \\ & f_{\cdot} = f_{\cdot} = f_{\cdot} = ... = \bullet \end{aligned}\right\}\ at\ y = -H\ , \tag{60}$$

$$\left.\begin{aligned} & u_{\cdot} = -\bullet\ ,\ u_{\cdot} = u_{\cdot} = ... = \bullet \\ & \theta_{\cdot} = \bullet\ ,\ \ \theta_{\cdot} = \theta_{\cdot} = ... = \bullet \\ & f_{\cdot} = \bullet\ ,\ f_{\cdot} = f_{\cdot} = ... = \bullet \end{aligned}\right\}\ at\ y = H$$

The initial approximations (zero order) of equations (56-58) were obtained as follows:

$$\left.\begin{aligned} u_{\cdot} &= \frac{S_{\cdot}}{\bullet} y^{\cdot} + S_{\cdot}\ , \\ \theta_{\cdot} &= \frac{B_{\cdot}}{\bullet} y^{\cdot} + B_{\cdot}y + B_{\cdot}\ , \\ f_{\cdot} &= E_{\cdot}y + E_{\cdot} \end{aligned}\right\}, \tag{61}$$

The computation of axial velocity u , temperature distribution θ, and nanoparticles concentration f includes both first and second-order solutions. However, it appears that some of the input parameters do not significantly affect the concentration. As a result, the concentration solution is enhanced up to the third order. After summing up all the computed values and substituting ω_0 with the value $\omega_{\cdot} = \bullet$, we obtain the following set of approximated solutions:

$$\begin{aligned} u(y) = {} & S_{\cdot\cdot} + S_{\cdot\cdot}y^{\cdot} + S_{\cdot\cdot}y^{\cdot} + S_{\cdot\cdot}y^{\cdot} + S_{\cdot\cdot}y^{\cdot} \\ & + S_{\cdot\cdot}y^{\cdot} + S_{\cdot\cdot}y^{\cdot\cdot} + S_{\cdot\cdot}Cosh[\Omega\, y] \\ & + y^{\cdot}(S_{\cdot\cdot} + S_{\cdot\cdot}Cosh[\Omega\, y]) \\ & + y^{\cdot}(S_{\cdot\cdot} + S_{\cdot\cdot}Sinh[\Omega\, y]) \\ & + y(S_{\cdot\cdot} + S_{\cdot\cdot}Sinh[\Omega\, y]) \end{aligned}\ , \tag{62}$$

$$\begin{aligned} T(y) = {} & B_{\cdot\cdot} + B_{\cdot\cdot}y^{\cdot} + B_{\cdot\cdot}y^{\cdot} + B_{\cdot\cdot}y^{\cdot} + B_{\cdot\cdot}y^{\cdot} \\ & + B_{\cdot\cdot}y^{\cdot} + B_{\cdot\cdot}y^{\cdot\cdot} + B_{\cdot\cdot}Cosh[\Omega\, y] \\ & + y^{\cdot}(B_{\cdot\cdot} + B_{\cdot\cdot}Cosh[\Omega\, y]) \\ & + y^{\cdot}(B_{\cdot\cdot} + B_{\cdot\cdot}Sinh[\Omega\, y]) \\ & + y(B_{\cdot\cdot} + B_{\cdot\cdot}Sinh[\Omega\, y]) \end{aligned}\ , \tag{63}$$

$$
\begin{aligned}
f(y) = {} & E_{\bullet\bullet} + E_{\bullet\bullet} y^{\bullet} + E_{\bullet\bullet} y^{\bullet} + E_{\bullet\bullet} y^{\bullet} \\
& + E_{\bullet\bullet} y^{\bullet} + E_{\bullet\bullet} y^{\bullet} + E_{\bullet\bullet} y^{\bullet\bullet} + E_{\bullet\bullet} y^{\bullet\bullet} \\
& + E_{\bullet\bullet} y^{\bullet\bullet} + E_{\bullet\bullet} y^{\bullet\bullet} + E_{\bullet\bullet} Cosh[\Omega y] \\
& + E_{\bullet\bullet} Sinh[\Omega y] + y \begin{pmatrix} E_{\bullet\bullet} + E_{\bullet\bullet} Cosh[\Omega y] \\ + E_{\bullet\bullet} Sinh[\Omega y] \end{pmatrix} . \\
& + y^{\bullet} \left(E_{\bullet\bullet} + E_{\bullet\bullet} Cosh[\Omega y] + E_{\bullet\bullet} Sinh[\Omega y] \right) \\
& + y^{\bullet} \left(E_{\bullet\bullet} + E_{\bullet\bullet} Cosh[\Omega y] + E_{\bullet\bullet} Sinh[\Omega y] \right) \\
& + y^{\bullet} \left(E_{\bullet\bullet} + E_{\bullet\bullet} Sinh[\Omega y] \right)
\end{aligned}
\tag{64}
$$

The constants $S_{\bullet} \to S_{\bullet\bullet}$, $B_{\bullet} \to B_{\bullet\bullet}$ and $E_{\bullet} \to E_{\bullet\bullet}$ are functions in the entering physical parameters and they are available upon request from the authors.

4. Results and Discussion

The governing equations for velocity, temperature, and concentration were effectively solved using the HPM method. In order to validate and reinforce the obtained results, the influence of different parameters relevant to the problem was examined and illustrated through corresponding figures (3) – (19). From a physical perspective, nanoparticles exhibit excellent heat conductivity. Consequently, to effectively account for their strong thermal diffusivity, the Prandtl number Pr is set to a small value. Additionally, [37] in the case of a thin electric double layer (EDL), the flow can be accurately approximated as unidirectional along the axis of the micro-channel. Thereby, the electroosmotic parameter $\left(\Omega = h\, z\, e \sqrt{\frac{2\, N_0}{\varepsilon\, k_B T_{av}}} = \frac{h}{\lambda_\alpha} \right)$ is set to a large value to emphasize the presence of a thin electric double layer (EDL). In addition, the skin friction coefficient τ_ω depends on the modified Darcy's parameter N. Considering low Reynolds number Re, it is found that unrealistic larges values of τ_ω ($\tau_\omega >= \bullet\bullet\bullet\bullet$) at $N > \bullet.\bullet\bullet$, so that N is taken in the range $[\bullet, \bullet.\bullet]$. Furthermore, in Eq. (41) since the dimensionless of θ and f depend on the difference $T_{\bullet} - T_{\bullet}$ and $C_{\bullet} - C_{\bullet}$, If we considered $T_{\bullet} > T_{\bullet}$ and $C_{\bullet} > C_{\bullet}$, hence the values of G_r, B_r, Ec, N_b, N_t and S should be positive and $\bullet < \beta < \bullet.\bullet\bullet$ to verify the condition $(\beta - \bullet) << \bullet$.

The figures are depicted for a system whose particulars are following dimensionless numbers:

$\partial p / \partial x = \bullet$, $N = \bullet.\bullet\bullet$, $G_r = \bullet.\bullet$, $G_c = \bullet.\bullet$, $k = \bullet.\bullet$, $U_{HS} = \bullet$, $\Omega = \bullet$, $S = \bullet.\bullet$, $\beta = \bullet.\bullet\bullet$, $N_t = \bullet.\bullet$, $N_b = \bullet.\bullet$, $Ec = \bullet$, $Pr = \bullet.\bullet$, $Q = \bullet$, $M = \bullet.\bullet$, $E = \bullet.\bullet$, $Sc = \bullet.\bullet$, $E_A = \bullet.\bullet$, $k_\alpha = \bullet.\bullet$, $n = \bullet$.

4.1 Velocity profile.

Figure (3) shows in the absence of porous medium $(k \to \infty)$ and $(N \to \bullet)$; the flow direction reverses and aligns with the positive direction of the x-axis.

Figure (4) shows that the axial velocity u increases (negativity decreases) as permeability k increases. This behavior is in agreement with Eldabe et al. [44]. Physically, as k increases the effect of permeability near the walls is enhanced, while the influence of the external force $(\bullet / k)$ diminishes around the middle of the tube. Assuming a no-slip condition (velocity fixed at the walls), the impact of the external force becomes predominant, resulting in increased resistance to the flow. Consequently, the net flow decreases along its flow direction (negative flow decreases).

Figure (5) shows that u decreases (negativity increases) as the modified Darcy term N increases. This suggests that in the presence of the modified Darcy medium, the influence of permeability extends to the core flow (middle of the tube), consequently enhancing the flow in the direction of its movement.

Figures (6) and (7) demonstrate contrasting effects of electro-osmotic parameter Ω on the axial velocity u. Figure (6) depicts that u increases (decreases in negativity) as Ω increases. The behavior exhibited here aligns with the findings of Chaube et al. [45], and Ramesh et al. [40]. On the other hand, in the absence of induced magnetic effect $(M = \bullet)$ and the modified Darcy effect $(N = \bullet)$. Figure (7) depicts u decreases (increases in negativity) as Ω increases. This behavior is in agreement with Abdelmoneim et al. [39] and Hegazy et al. [46]. Physically the wall in contact with the electrolyte solution acquires an electric charge. This charged surface attracts cations (positively charged ions) while repelling anions (negatively charged ions). Upon the application of an electric field, the mobile cations near the wall, within the diffuse layer of the Electric Double Layer (EDL), migrate towards the cathode, simultaneously inducing the bulk fluid to move in that direction (resulting in Electrophoretic or Electroosmotic Flow, EOF). Hence, the EOF is in the positive direction of X-axis [47]. Furthermore, the electro-osmotic parameter Ω is inversely proportional to the length of electric double layer

(Debye length), so as Ω increases the Debye length decreases and the diffuse layer diminishes. As a result, this reduces the impact of the electro-osmotic flow (EOF). So that the net flow increases along the flow directions (negativity increases). On the contrary, figure (6) depicts that in the presence of induced magnetic effect and the modified Darcy effects the direction of EOF is reversed and EOF supports the net flow in the negative direction. Hence as EOF decreases the net flow decreases in its negativity.

Figure (8) shows that u decreases (negativity increases) as the magnetic parameter M increases, this behavior is in agreement with Ishtiaq [32], Noreen et al. [35] and Ramesh et al. [40]. Physically, the magnetic field acts perpendicular to the flow, thereby opposing and resisting the flow in that transverse direction. This resistance is governed by the Lorentz force, which ultimately diminishes the flow along the positive direction of the y-axis.

Figure (9) depicts that u decreases (negativity increases) as thermal Grashof number G_r increases. This agrees with Mohamed and Abozeid [48]. Physically, Gr represents the ratio of the buoyancy force across fluid layers to the viscous force acting on those layers. As Grashof number increases, it signifies a reduction in viscosity, consequently leading to smoother fluid flow in the direction of flow.

4.2 Temperature profile.

The graphs of the temperature θ satisfy the boundary conditions (53) and depicts that θ gradually decreases till a definite value (the peak of the curve is minimum point), after which it starts increasing once again. Physically, heat transfer occurs between the fluid and the surrounding walls to reach an equilibrium state. Considering the temperature at the right wall is higher than that at the left wall $(T_{\bullet} - T_{\bullet} > \bullet)$. In addition, as evident from Eq. (41), θ depends on the temperature difference between the fluid layers and the left wall. Considering $(T - T_{\bullet} > \bullet)$; near the left wall, the fluid layers undergo cooling until it reaches a minimum temperature point before heating up again towards the right wall. Thereby, the temperature distribution takes on a reverse shape along the path from left wall $(y = -H)$to the right wall $(y = H)$. In other words, θ increases in the negative direction of the Y-axis.

Figure (10) illustrates that the temperature θ decreases (in the positive direction of Y-axis) as thermal Grashof number G_r increases. This result is in agreement with Eldabe et al [20], Mustafa et al. [49] and Ibrahim et al [50]. Physically, in the context of natural convection heat transfer, thermal Grashof number G_r represents the ratio between the buoyancy force resulting from variations in fluid density (caused by temperature differences) and the viscous force acting on the fluid layers [3]. This means that as G_r increases the buoyancy force becomes more pronounced, leading to a significant improvement in heat transfer through convection. During the cooling process near the left wall, the hotter fluid layers are forced to move to the left side and exchange places with colder layers. Conversely, in the heating process near the right wall, the hotter fluid layers are pulled towards the middle of the tube (pulled to the left side) to be replaced by colder layers. As a result, in both regions, a greater number of hotter layers are driven to the left side, leading to an increase in temperature along the negative direction of the y-axis. The explanation provided here is consistent with the findings of Mansour and Abozeid [51] Ismael al. [52].

Figure (11) shows that θ increases (in the positive direction of Y-axis) as the thermophoresis parameter N_t increases, this behavior is in agreement with Abdelmoneim et al. [39], Eldabe et al. [53], Abozeid and Mohamed [54], and Abozeid et al [55]. In physical terms, the increase in N_t signifies an enhancement in the thermophoresis force, which drives nanoparticles from the hot region (right wall) to the cold region (left wall) [39]. Since the nanoparticles are good conductors of heat, therefore it plays a crucial role in the temperature distribution within the system. Since the flow of the nanoparticles along the negative direction of the y-axis is enhanced. Thereby; the temperature distribution along the negative direction of the y-axis should be enhanced. This effect is particularly noticeable as the minimum temperature peak becomes more negative.

4.3 Concentration profile.

Figure (12) shows that as Schmidt number Sc increases f increases. This behavior is in agreement with Abozeid and Mohamed [54], Sheikholeslami and Ganji [56], and Hayat et al. [57]. Physically, Schmidt number represents the ratio of momentum diffusivity (kinematic viscosity) and mass diffusivity. Hence, the as Sc increases the mass diffusivity (spread of the nanoparticles) decreases, leading to an increase in concentration.

Figure (13) demonstrates that f increases with an increase in the Chemical reaction parameter k_α. In a physical sense, as the chemical reaction rate increases, a greater number of new chemical products are formed, leading to a decrease in the concentration of the reactants (nanoparticles).

Figure (14) illustrates that f decreases as the activation parameter E_A increase. In the realm of

physical chemistry, the activation energy signifies the minimum amount of energy necessary to initiate a chemical reaction.
The Arrhenius equation elucidates the inverse relationship that exists between activation energy and the reaction rate parameter. Thus, when activation energy rises, the reaction rate parameter decreases, and conversely. Hence, higher activation energy generally results in a slower reaction rate, so that figure (14) matches with figure (13).

Figure (15) illustrates that f increases as the magnetic parameter M increase. This effect plays an important role in many biological applications such as magnetic resonance imaging contrast enhancement, tissue repair, drug delivery, and cell separation [58]. In the review article of Pankhurst et al. [59] the flow of nanofluid in the presence of external magnetic field is used in the treatment of tumour cells. By situating a magnet outside the body, the nanoparticles tend to concentrate more within the bloodstream when exposed to high-gradient magnetic fields (as seen in figure 16). Once the drug/carrier is concentrated at the target, the drug is released and absorbed up by the tumour cells.

Figure (17) illustrates that f decreases as the induced electric field parameter E increase. This suggests that as the induced electric field strength increases the nanoparticles disperse through the fluid (concentration decreases)
The discussions for the rest of the figures are omitted to save space and avoid repetition (increase-decrease).

4.4 skin friction and Nusselt Number.

Skin friction, also known as shear stress or wall shear stress, plays a crucial role in fluid mechanics and has valuable physical importance in various applications. It refers to the force per unit area that the fluid exerts on a solid surface as it flows past that surface. As the Skin friction (frictional force) increases, greater energy is required to transport a fluid along the length of the channel. The skin friction coefficient τ_ω quantifies the resistance force. Furthermore, when accounting for the "no-slip" condition (where solid walls remain stationary in the moving frame), the skin friction coefficient typically assumes a positive value. This implies that the frictional force acts counter to the flow velocity's direction, serving to decelerate the fluid.

Figure 18 illustrates that an increase in the electroosmotic parameter Ω results in an increase in the skin friction coefficient τ_ω. This behavior agrees with Ahmed et al. [60]. Physically, as mentioned before, when Ω increases the diffuse layer diminishes. Consequently, the strong electrostatic force becomes more pronounced, thereby reinforcing the frictional force near the walls.

Heat transfer by convection occurs when a fluid passes over a solid surface in the presence of a temperature difference between them. Nusselt number Nu is the dimensionless parameter that characterizes the convective heat transfer rate between a fluid and a solid surface, serving as a measure of how efficiently heat is transferred through convection.

Figure (19) shows that Nusselt number Nu increases as the Prandtl number Pr increases. Physically, the behavior of the Nusselt number strongly depends on Pr. In addition, positive Nusselt numbers indicate that heat consistently transfers from the fluid to the plate [61]. As Pr increases, thermal diffusivity decreases. Consequently, convection becomes a more dominant mode of heat transfer compared to conduction, leading to an increase in the Nusselt number.

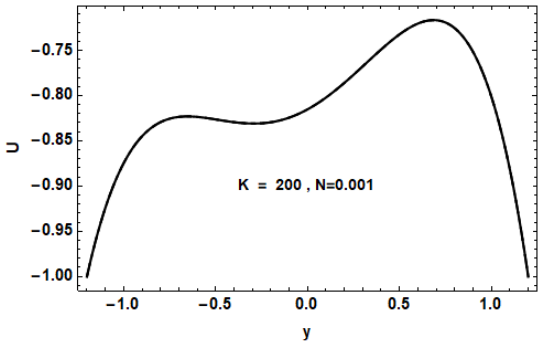

Figure 3: The velocity distribution u is plotted with y, at values of $k = \bullet\bullet\bullet$ and $N = \bullet.\bullet\bullet\bullet$.

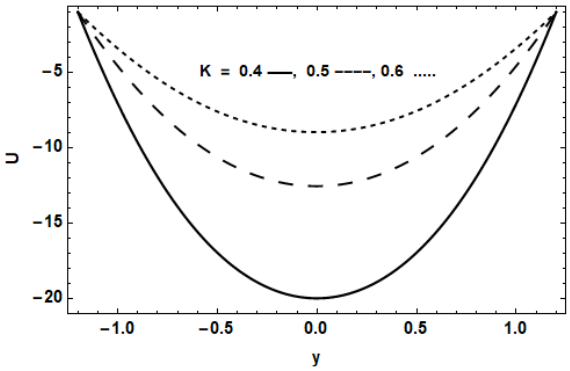

Figure 4: The velocity distribution u is plotted with y for different values of k.

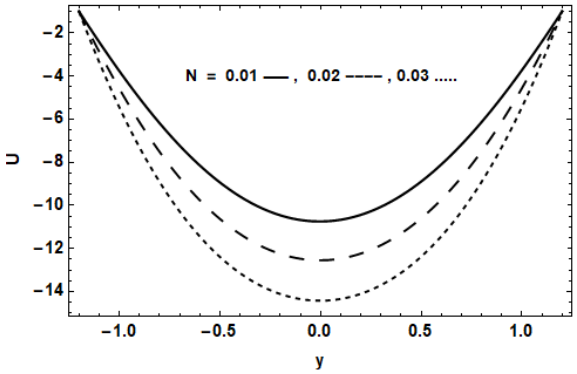

Figure 5: The velocity distribution u is plotted with y for different values of N.

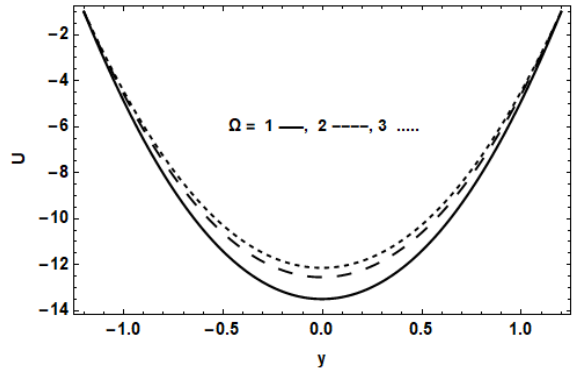

Figure 6: The velocity distribution u is plotted with y for different values of Ω.

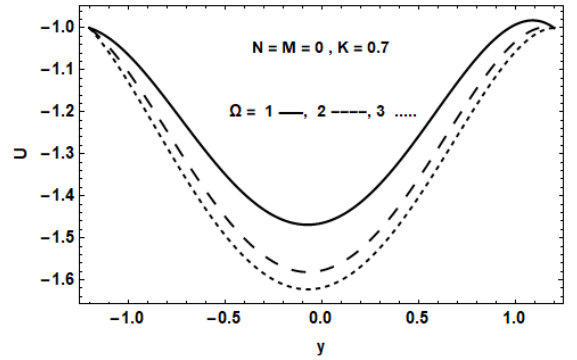

Figure 7: The velocity distribution u is plotted with y for different values of Ω.

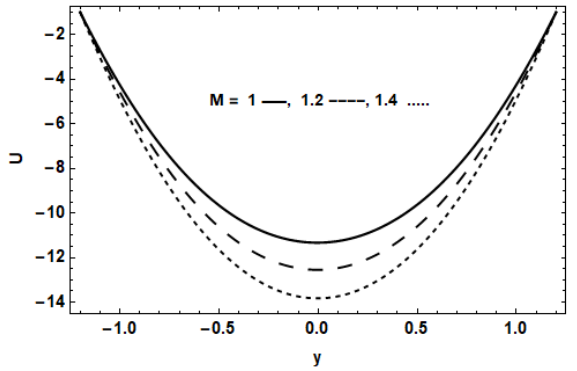

Figure 8: The velocity distribution u is plotted with y for different values of M.

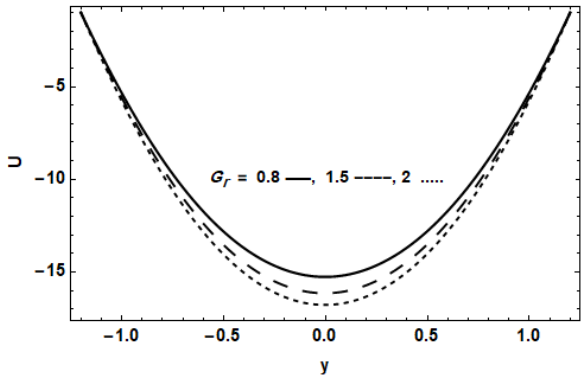

Figure 9: The velocity distribution u is plotted with y for different values of G_r.

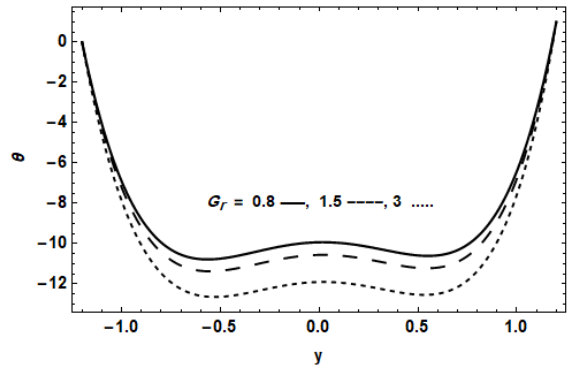

Figure 10: The temperature distribution θ is plotted with y for different values of G_r.

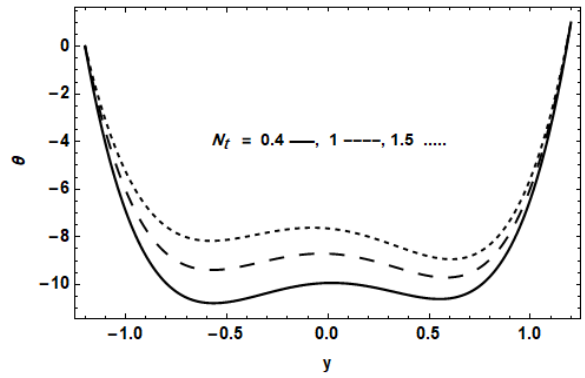

Figure 11: The temperature distribution θ is plotted with y for different values of N_t.

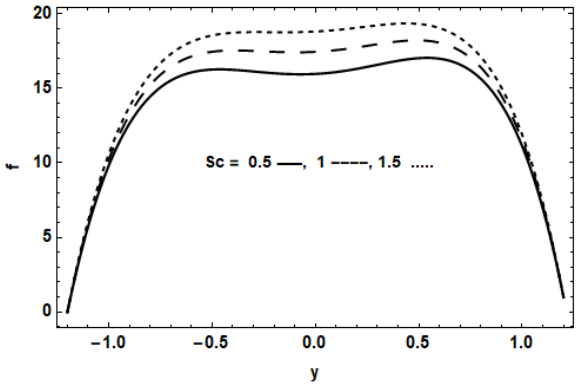

Figure 12: The nanoparticle concentration f is plotted with y for different values of S_c.

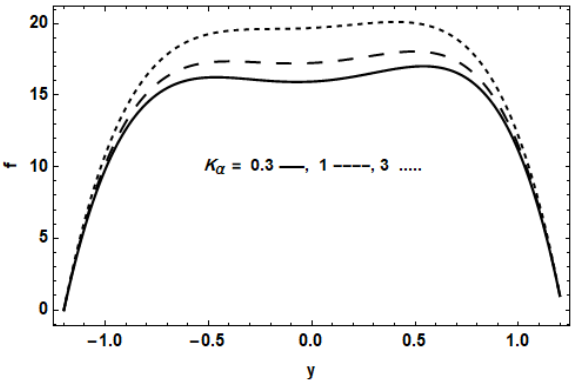

Figure 13: The nanoparticle concentration f is plotted with y for different values of K_α.

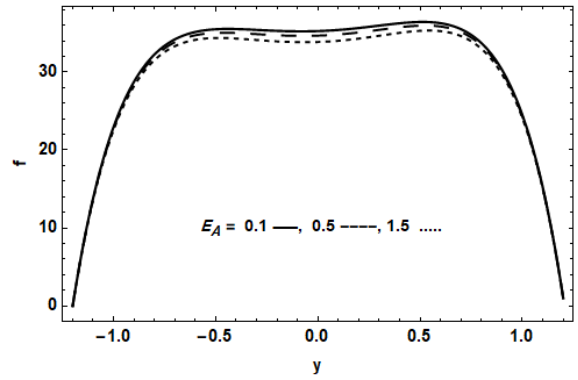

Figure 14: The nanoparticle concentration f is plotted with y for different values of E_A.

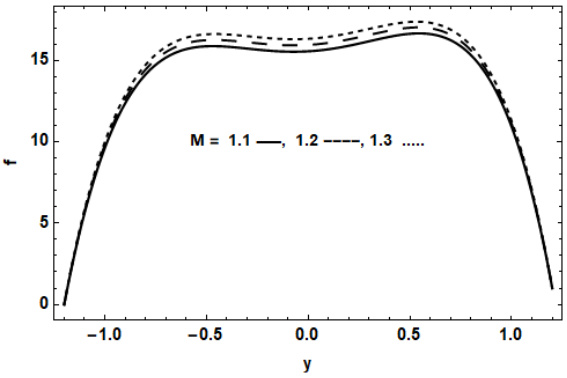

Figure 15: The nanoparticle concentration f is plotted with y for different values of M.

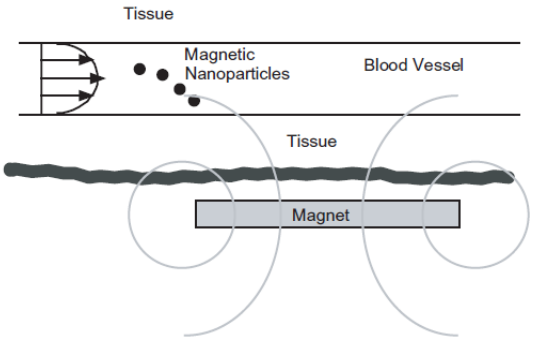

Figure 16: magnetic drug delivery system depicted in cross-section [59].

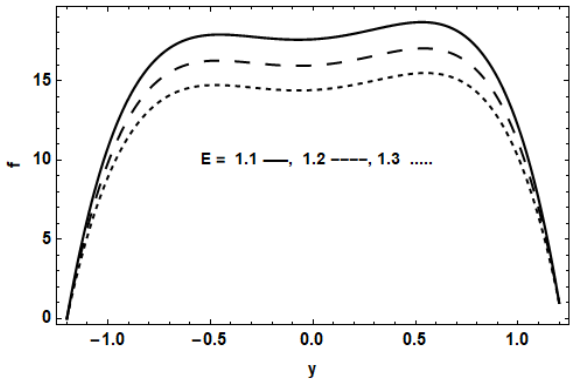

Figure 17: The nanoparticle concentration f is plotted with y for different values of E.

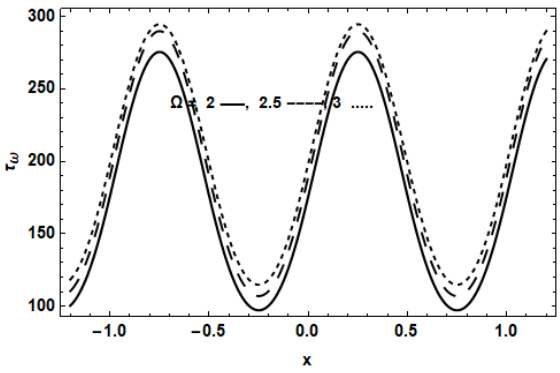

Figure 18: skin friction coefficient τ_ω is plotted with x for different values of Ω .

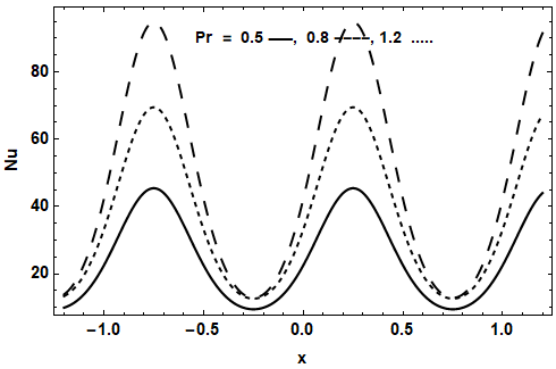

Figure 19: Nusselt number Nu is plotted with x for different values of Pr .

Table 1: Comparison between the present work and Eldabe et al. [62] for various values of k and M

k $(k \equiv D_a)$	M	τ_ω in the present work	τ_ω as calculated from the work Eldabe et al. [62]
0.5	1.2	13.006	13.056
0.45	1.2	15.694	15.694
0.5	1.3	14.174	14.180
0.45	1.3	17.022	17.020

Since Eldabe et al. [62] got an analytical solution for the axial velocity and mentioned the constants in the appendix. In addition, in our work when $N = G_r = G_c = U_{HS} = E = \bullet$, and in the work of Eldabe et al. [62] when $m = \bullet$ the two works are close to each other. The numerical values for the skin friction coefficient, $\tau_\omega(x)|_{x=\bullet}$ are calculated in both works for various values of. It is clear M and k from Table 1 that the behavior of τ_ω in our work approaches it in Abbas et al. [3].

5. Conclusion

The primary objective of this research is to introduce a mathematical model that examines the MHD (Magnetohydrodynamic) peristaltic flow of a third-grade model while considering the influence of electromagnetic field (EMF). The fluid flow takes place within a symmetrical vertical channel filled with a porous medium that adheres to a modified Darcy model. Furthermore, this investigation considers several significant factors, including mixed convection, viscous dissipation, heat generation and chemical reactions with activation energy.

The primary findings of this study are as follows:

1. The presence of the modified Darcy term significantly amplifies the influence of the permeability of the medium within the middle of the tube. As a result the fluid flow is much easier in the middle of the tube.
2. A notable correlation exists between the electric double layer (EDL) and the permeability of the medium. This relationship arises from the formulation of the EDL adjacent to the walls (high porous region). Nonetheless, this effect becomes negligible in the presence of the modified Darcy term.
3. In the absence of porous medium $(k \to \infty)$ and $(N \to \bullet)$, the fluid flows in the positive direction of the x-axis.
4. An increase in the thermal Grashof number G_r results in a flow direction of the hot layers towards the low-temperature wall. So, in the case of the reverse shape of the temperature distribution, as the thermal Grashof number G_r increases, the flow of the hot layers moves in the negative direction of the y-axis, causing a rise in temperature in that direction.
5. The investigation reveals that both the activation energy and the Brownian motion parameter have similar effects on the concentration profile, as they both lead to a decrease in concentration.
6. The second-order solution for the concentration does not account for the impact of mixed convection on the concentration. Therefore, to consider this effect, the solution is elevated to the third order.
7. Nano particles concentration can be enhanced be increasing the strength of the external magnetic field, this effect can be noticed in many biological applications such as drug delivery.
8. The nanoparticles concentration is affected in opposite ways by increasing each of the

Brownian motion parameter N_b and the thermophoresis parameter N_t.

9. The peristaltic flow of non-Newtonian fluids offers valuable applications in the realms of medicine and engineering, as documented in references [63-69]. These applications span various sectors, including:

- Utilization in the chemical processing industry and plastics processing industry.
- Transfer of fuels and lubricants
- Drug delivery and tumor therapy.

Acknowledgments
The authors thank the reviewers for their valuable comments, which improved and enriched their manuscript.

Nomenclature

	Roman Symbols	**SI Units**
a	The amplitude of the wave	m
A	Chemical reaction rate	mol/(m^3 · s)
$\lvert\vec{A}.\rvert$	Shear strain	–
$\bar{c}$	The wave velocity	m s^{-1}
D_B	Brownian diffusion coefficient	–
D_T	Thermophoretic diffusion coefficient	–
e	The electronic charge.	The elementary charge "e"
E	Dimensionless strength of the induced electric field	–
Ec	Eckert number	–
E_A	Dimensionless Activation energy parameter	–
$H(x)$	transverse vibration of the wall	–
$H.$	External magnetic field strength	T (tesla)
K	Thermal conductivity	W m^{-1} K^{-1}
k	Permeability constant	H (Henry)/m
k_B	Boltzmann constant	–
k_α	Dimensionless Chemical reaction parameter	–
M	Dimensionless magnetic parameter	–
n	Fitted rate constant	s^{-}1
N	Dimensionless modified Darcy's parameter	–
$N.$	Bulk volume concentration for positive or negative ions	mol/m³
N_b	Brownian motion parameter	–
N_T	Thermophoresis parameter	–
P	The fluid pressure	Kg m^{-1} s^{-2}
Pr	Prandtl number	–
Re	Reynolds number	–
R_x, R_y	modified Darcy's components	–
R_m	Magnetic Reynolds number	–
$Q.$	The volumetric rate of heat	m^3 s^{-1}

Sc	Schmidt number	–
$T_{\bullet}$, $T_{\bullet}$	The temperature distribution in the fixed and the moving frames	K (Kelvin)
T_{av}	Local absolute temperature	K (Kelvin)
U_{HS}	The dimensionless Helmholtz-Smoluchowski velocity	–
x	Axial coordinate	m
y	Transverse coordinate	m
z	The valence number of ions.	–
	Greek symbols	
α_i , β_i $i = \bullet, \bullet, \bullet$	Material constants	–
$\theta(y)$	The dimensionless fluid temperature	–
ϕ	Electric potential for EDL (Zeta potential)	Volts (V)
ζ	Zeta potential at the right wall	Volts (V)
Ω	Electroosmotic parameter	–
μ_0	Dynamic viscosity of fluid	(Pa·s) or N·s/m²
μ	apparent viscosity of fluid	(Pa·s) or N·s/m²
ρ_e	Density of the total ionic energy	Joules per cubic meter (J/m³).
ε	Electric permittivity	Farads per meter (F/m).
n^+	The number of density of cations	m⁻³
n^-	The number of density of anions	m⁻³
λ	Wavelength	m
λ_α	The thickness of EDL (Debye length)	m
ρ_f	The density of the fluid	kg/m³
ρ_P	The density of the particle	kg/m³
$\theta(y)$	The dimensionless fluid temperature	–
$(\rho c)_f$	Heat capacity of the fluid	Joules per kelvin per kilogram (J/(K·kg)).
$(\rho c)_P$	Effective heat capacity of the nanoparticle's material	Joules per kelvin per kilogram (J/(K·kg)).

References

1. K.R. Aglawe, R.K. Yadav, S.B. Thool, "Preparation, applications, and challenges of nanofluids in electronic cooling, A systematic review," Materials Today Proceedings, 43, 366–372 (2021).
2. S.A. Hussein, N.T. Eldabe, "Peristaltic pumping of Boron Nitride-Ethylene Glycol nanofluid through a complex wavy micro-channel under the effect of induced magnetic field and double diffusive," Scientific Reports, 13, 2622 (2023).
3. N.T. El-dabe, M.Y. Abou-zeid, M.A. Mohamed, M. Maged, "Peristaltic flow of Herschel Bulkley nanofluid through a non-Darcy porous medium with heat transfer under slip condition," International Journal of Applied Electromagnetics and Mechanics, 66, 649–668 (2021).
4. Abuiyada, A., Eldabe, N., Abouzeid, M., Elshaboury, S.: Influence of Both Ohmic

Dissipation and Activation Energy on Peristaltic Transport of Jeffery Nanofluid through a Porous Media. CFD Lett. **15**, 65–85 (2023)

5. Y. Mohamed, N.T. Eldabe, M. Abouzeid, M.E. Ouaf, D. Mostapha, "Chemical Reaction and Thermal Radiation via Cattaneo-Christov Double Diffusion (CCDD) Effects on Squeezing Non-Newtonian Nanofluid Flow between Two–Parallel Plates," Egyptian Journal of Chemistry, 66, 209–231 (2023).
6. N.T. Eldabe, S.M. El Shaboury, H.A. El Arabawy, M.Y. Abou-zeid, A. Abuiyada, "Wall properties and Joule heating effects on MHD peristaltic transport of Bingham non-Newtonian nanofluid," International Journal of Applied Electromagnetics and Mechanics, 69(1), 87–106 (2022).
7. N.T. Eldabe, M. Abouzeid, D. Roshdy, Y. Mohamed, M.E. Ouaf, "Impacts of Chemical Reaction and Electric Field with Cattaneo–Christov Theories on Peristaltic Transport of a Hyperbolic Micropolar Nanofluid," Egyptian Journal of Chemistry, 66, 63–85 (2023).
8. M.E. Ouaf, M. Abou-zeid, Y.M. Younis, "Entropy generation and chemical reaction effects on MHD non-Newtonian nanofluid flow in a sinusoidal channel," International Journal of Applied Electromagnetics and Mechanics, 69(1), 45–65 (2022).
9. A.M. Ismael, N.T. Eldabe, M. Y. Abouzeid, S.M. El Shabouri, "Thermal micropolar and couple stresses effects on peristaltic flow of biviscosity nanofluid through a porous medium," Scientific Reports, 12, 1–14 (2022).
10. N. T. Eldabe, G. M. Moatimid, M. Y. Abouzeid, A. A. ElShekhipy, N. F. Abdallah, "A semianalytical technique for MHD peristalsis of pseudoplastic nanofluid with temperature-dependent viscosity: Application in drug delivery system," Heat Transfer-Asian Research, 49(1), 424–440 (2020).
11. Y. Mostafa, N. El-Dabe, M. Abou-Zeid, M. Oauf, D. Mostapha, "Peristaltic Transport of Carreau Coupled Stress Nanofluid with Cattaneo-Christov Heat Flux Model Inside a Symmetric Channel," Journal of Advanced Research in Fluid Mechanics and Thermal Sciences, 98(1), 1-17 (2022).
12. A.S. Kotnurkar, N. Kallolikar, E.N. Thabet, "Double-diffusive bioconvection effects on multi-slip peristaltic flow of Jeffrey nanofluid in an asymmetric channel," Pramana, 97, 108 (2023).
13. N.T. Eldabe, S.M. El Shabouri, T.N. Salama, A.M. Ismael, "Ohmic and viscous dissipation effects on micropolar non-Newtonian nanofluid Al 2O 3 flow through a non-Darcy porous media," International Journal of Applied Electromagnetics and Mechanics, 68, 209–221 (2022).
14. N. El-Dabe, M.Y. Abou-Zeid, M.E. Oauf, D.R. Mostapha, Y.M. Mohamed, "Cattaneo–Christov heat flux effect on MHD peristaltic transport of Bingham Al2O3 nanofluid through a non-Darcy porous medium," International Journal of Applied Electromagnetics and Mechanics, 68, 59–84 (2022).
15. Abuiyada, A., Eldabe, N.T., Abouzeid, M., Elshaboury, S.: Significance of Heat Source and Activation Energy on MHD Peristaltic Transport of Couple Stress Hyperbolic Tangent Nanofluid through an Inclined Tapered Asymmetric Channel. Egypt. J. Chem. **66**, 417–436 (2023)
16. N.T. Eldabe, G.M. Moatimid, M. Abouzeid, A. Abdelhafeez, "Instantaneous thermal-diffusion and diffusion-thermo effects on Carreau nanofluid flow over a stretching porous sheet," Journal of Advanced Research in Fluid Mechanics and Thermal Sciences, 72, 142–157 (2020).
17. M.Y. Abou-Zeid, "Implicit Homotopy Perturbation Method for MHD Non-Newtonian Nanofluid Flow with Cattaneo-Christov Heat Flux Due to Parallel Rotating Disks," Journal of Nanofluids, 8, 1648–1653 (2019).
18. N.T. Eldabe, M. Abouzeid, H.A. Shawky, "MHD peristaltic transport of Bingham blood fluid with heat and mass transfer through a non-uniform channel," Journal of Advanced Research in Fluid Mechanics and Thermal Sciences, 77, 145–159 (2021).
19. N.T. Eldabe, M.Y. Abou-zeid, A.S.A. Seliem, A.A. Elenna, N. Hegazy, "Thermal diffusion and diffusion thermo effects on magnetohydrodynamics transport of non-Newtonian nanofluid through a porous media between two wavy co-axial tubes," IEEE Transactions on Plasma Science, 50, 1282–1290 (2022).
20 N.T.M. El-Dabe, M.Y. Abou-zeid, M.A.A. Mohamed, M.M. Abd-Elmoneim, "Peristaltic Mixed Convection Slip Flow of a Bingham Nanofluid Through a Non-Darcy Porous Medium in an Inclined Non-Uniform Duct with Viscous Dissipation and Radiation," Journal of Applied Nonlinear Dynamics, 12, 231–243 (2023).

21. Y. Akbar, S. Huang, M.U. Ashraf, K.S. Nisar, M.M. Alam, "Electrothermal analysis for reactive Powell Eyring nanofluid flow regulated by peristaltic pumping with mass transfer," Case Studies in Thermal Engineering, 44, 102828 (2023).
22. N. Eldabe, M. Abouzeid, H. Ali, "Effect of heat and mass transfer on Casson fluid flow between two co-axial tubes with peristalsis," Journal of Advanced Research in Fluid Mechanics and Thermal Sciences, 76, 54–75 (2020).
23. P.A. Davidson, "An introduction to magnetohydrodynamics," Cambridge University Press, New York, Chapter 5, 117 (2002).
24. M.G. Ibrahim, M.Y. Abou-Zeid, "Influence of variable velocity slip condition and activation energy on MHD peristaltic flow of Prandtl nanofluid through a non-uniform channel," Scientific Reports, 12, 18747 (2022).
25. M. Ouaf, M. Abouzeid, M.G. Ibrahim, "Effects of both variable electrical conductivity and microstructural/multiple slips on MHD flow of micropolar nanofluid," Egyptian Journal of Chemistry, 66, 449–456 (2023).
26. A.J. Abuiyada, N.T. Eldabe, M.Y. Abou-zeid, S.M. El Shaboury, "Effects of thermal diffusion and diffusion thermo on a chemically reacting MHD peristaltic transport of Bingham plastic nanofluid," Journal of Advanced Research in Fluid Mechanics and Thermal Sciences, 98, 24–43 (2022).
27. N.T. Eldabe, R.R. Rizkalla, M.Y. Abou-Zeid, V.M. Ayad, "Effect of induced magnetic field on non-Newtonian Al2O3 nanofluid motion through a boundary-layer with gyrotactic microorganisms," Thermal Science, 26, 411–422 (2022).
28. M. Abouzeid, "Chemical reaction and non-Darcian effects on MHD generalized Newtonian nanofluid motion," Egyptian Journal of Chemistry, 65, 647–655 (2022).
29. N.T. Eldabe, O.M. Abo-Seida, A.E. Abd El Naby, M. Ibrahim, "Effects of bivariation viscosity and magnetic field on trapping in a uniform tube with peristalsis," Information Sciences Letters, 11, 1945–1954 (2022).
30. N.T.M. Eldabe, M.F. El-Sayed, A.Y. Ghaly, H.M. Sayed, "Peristaltically induced transport of a MHD biviscosity fluid in a non-uniform tube," Physica A: Statistical Mechanics and its Applications, 383, 253–266 (2007).
31. T. Hayat, A. Afsar, M. Khan, S. Asghar, "Peristaltic transport of a third order fluid under the effect of a magnetic field," Computers and Mathematics with Applications, 53, 1074–1087 (2007).
32. T. Hayat, Y. Khan, K.S. Mekheimer, N. Ali, "Effects of an induced magnetic field on the peristaltic flow of a third-order fluid," Numerical Methods for Partial Differential Equations: An International Journal, 26, 345–366 (2010).
33. F. Ishtiaq, R. Ellahi, M.M. Bhatti, S.Z. Alamri, "Insight into thermally radiative cilia-driven flow of electrically conducting non-Newtonian Jeffrey fluid under the influence of an induced magnetic field," Mathematics, 10, 2007 (2022).
34. K.S. Mekheimer, "Effect of the induced magnetic field on peristaltic flow of a couple stress fluid," Physics Letters A, 372, 4271–4278 (2008).
35. S. Noreen, T. Hayat, A. Alsaedi, "Study of slip and induced magnetic field on the peristaltic flow of pseudoplastic fluid," International Journal of Physical Sciences, 6, 8018–8026 (2011).
36. N.T. Eldabe, R.R. Rizkalla, M.Y. Abou-Zeid, V.M. Ayad, "Effect of induced magnetic field on non-Newtonian nanofluid Al2O3 motion through boundary-layer with gyrotactic microorganisms," Thermal Science, 26, 411–422 (2022).
37. D.L. House, "Ph.D. Thesis, Faculty of the Graduate School of Vanderbilt University" (2012).
38. S. Chakraborty, "Augmentation of peristaltic microflows through electro-osmotic mechanisms," Journal of Physics D: Applied Physics, 39(24), 5356 (2006).
39. M. Abdelmoneim, N.T. Eldabe, M.Y. Abouzeid, M.E. Ouaf, "Both modified Darcy's law and couple stresses effects on electro-osmotic flow of non-Newtonian nanofluid with peristalsis," International Journal of Applied Electromagnetics and Mechanics, 72(3), 1–25 (2023).
40. K. Ramesh, M. Rawal, A. Patel, "Numerical simulation of radiative MHD Sutterby nanofluid flow through porous medium in the presence of hall currents and electroosmosis," International Journal of Applied and Computational Mathematics, 7, 1–12 (2021).
41. S. Das, B. Barman, "Ramification of hall and ion-slip currents on electro-osmosis of ionic hybrid nanofluid in a peristaltic microchannel," Bionanoscience, 12, 957–978 (2022).

42. F. Carapau, P. Correia, L.M. Grilo, "Specific shear-dependent viscoelastic third-grade fluid model," AIP Conference Proceedings, 1790(1), 140008 (2016).
43. T. Hayat, S. Noreen, N. Ali, "Effect of an induced magnetic field on the peristaltic motion of Phan-Thien-Tanner (PTT) fluid," Zeitschrift für Naturforschung A, 65, 665–676 (2010).
44. N.T.M. Eldabe, M.A. Hassan, M.Y. Abou-Zeid, "Wall properties effect on the peristaltic motion of a coupled stress fluid with heat and mass transfer through a porous medium," Journal of Engineering Mechanics, 142, 4015102 (2016).
45. M.K. Chaube, A. Yadav, D. Tripathi, O.A. Bég, "Electroosmotic flow of biorheological micropolar fluids through microfluidic channels," Korea-Australia Rheology Journal, 30, 89–98 (2018).
46. N. Hegazy, N.T. Eldabe, M. Abouzeid, A. Abousaleem, A. Alana, "Influence of both chemical reaction and electro-osmosis on MHD non-Newtonian fluid flow with gold nanoparticles," Egyptian Journal of Chemistry (2023). [DOI: 10.21608/ejchem.2023.190175.7526]
47. A. Alizadeh, W. Hsu, M. Wang, H. Daiguji, "Electroosmotic flow: From microfluidics to nanofluidics," Electrophoresis, 42, 834–868 (2021).
48. M.A.A. Mohamed, M.Y. Abou-zeid, "MHD peristaltic flow of micropolar Casson nanofluid through a porous medium between two co-axial tubes," Journal of Porous Media, 22 (2019).
49. M. Mustafa, S. Abbasbandy, S. Hina, T. Hayat, "Numerical investigation on mixed convective peristaltic flow of fourth grade fluid with Dufour and Soret effects," Journal of Taiwan Institute of Chemical Engineers, 45, 308–316 (2014).
50. M.G. Ibrahim, N.F. Abdallah, M.Y. Abou-Zeid, "Activation energy and chemical reaction effects on MHD Bingham nanofluid flow through a non-Darcy porous media," Egyptian Journal of Chemistry, 65, 137–144 (2022).
51. H.M. Mansour, M.Y. Abou-Zeid, "Heat and mass transfer effect on non-Newtonian fluid flow in a non-uniform vertical tube with peristalsis," Journal of Advanced Research in Fluid Mechanics and Thermal Sciences, 61, 44–62 (2019).
52. A.M. Ismael, N.T. Eldabe, M.Y.A. Zeid, S.M. El Shabouri, "Entropy generation and nanoparticles CuO effects on MHD peristaltic transport of micropolar non-Newtonian fluid with velocity and temperature slip conditions," Egyptian Journal of Chemistry, 65(9), 715–722 (2022).
53. N.T. Eldabe, M.Y. Abou-zeid, A. Abosaliem, A. Elenna, N. Hegazy, "Homotopy perturbation approach for Ohmic dissipation and mixed convection effects on non-Newtonian nanofluid flow between two co-axial tubes with peristalsis," International Journal of Applied Electromagnetics and Mechanics, 67, 153–163 (2021).
54. M.Y. Abou-zeid, M.A.A. Mohamed, "Homotopy perturbation method for creeping flow of non-Newtonian power-law nanofluid in a nonuniform inclined channel with peristalsis," Zeitschrift für Naturforschung A, 72, 899–907 (2017).
55. M.Y. Abou-Zeid, A.A. Shaaban, M.Y. Alnour, "Numerical treatment and global error estimation of natural convective effects on gliding motion of bacteria on a power-law nanoslime through a non-Darcy porous medium," Journal of Porous Media, 18, (2015).
56. M. Sheikholeslami, D.D. Ganji, "Unsteady nanofluid flow and heat transfer in presence of magnetic field considering thermal radiation," Journal of the Brazilian Society of Mechanical Sciences and Engineering, 37, 895–902 (2015).
57. T. Hayat, A.A. Khan, F. Bibi, S. Farooq, "Activation energy and non-Darcy resistance in magneto peristalsis of Jeffrey material," Journal of Physics and Chemistry of Solids, 129, 155–161 (2019).
58. A.K. Gupta, M. Gupta, "Synthesis and surface engineering of iron oxide nanoparticles for biomedical applications," Biomaterials, 26, 3995–4021 (2005).
59. Q.A. Pankhurst, J. Connolly, S.K. Jones, J.J.J. Dobson, "Applications of magnetic nanoparticles in biomedicine," Journal of Physics D: Applied Physics, 36, R167 (2003).
60. O.S. Ahmed, N.T. Eldabe, M.Y. Abou-Zeid, O.H. El-Kalaawy, S.M. Moawad, "Numerical treatment and global error estimation for thermal electro-osmosis effect on non-Newtonian nanofluid flow with time periodic variations," Scientific Reports, 13, 14788 (2023).
61. J. Prathap Kumar, J.C. Umavathi, "Free Convective Flow in an Open-Ended Vertical Porous Wavy Channel with a Perfectly Conductive Thin Baffle," Heat Transfer Research, 44, 227–256 (2015).

62. N.T.M. Eldabe, A.Y. Ghaly, S.N. Sallam, K. Elagamy, Y.M. Younis, "Hall effect on Peristaltic flow of a third-order fluid in a porous medium with heat and mass transfer," Journal of Applied Mathematics and Physics, 3, 1138 (2015).
63. A.A. Shaaban, M.Y. Abou-Zeid, "Effects of heat and mass transfer on MHD peristaltic flow of a non-Newtonian fluid through a porous medium between two coaxial cylinders," Mathematical Problems in Engineering, 2013, (2013).
64. N.T. Eldabe, M.Y. Abou-Zeid, O.H. El-Kalaawy, S.M. Moawad, O.S. Ahmed, "Electromagnetic steady motion of Casson fluid with heat and mass transfer through porous medium past a shrinking surface," Thermal Science, 25, 257–265 (2021).
65. N.T. Eldabe, M.Y. Abou-Zeid, "The wall properties effect on peristaltic transport of micropolar non-Newtonian fluid with heat and mass transfer," Mathematical Problems in Engineering, 2010, (2010).
66. N.T.M. El-dabe, M.Y. Abou-zeid, Y.M. Younis, "Magnetohydrodynamic peristaltic flow of Jeffry nanofluid with heat transfer through a porous medium in a vertical tube," Applied Mathematics and Information Sciences, 11, 1097–1103 (2017).
67. Abou-zeid, M.Y., Ouaf, M.E..: Effects of thermophoresis and mixed convection on Carreau fluid flow with gold nanoparticles. Egypt. J. Chem. 66, 2191 - 2200 (2023)
68. HA. Sayed and M.Y. Abouzeid, Radially varying viscosity and entropy generation effect on the Newtonian nanofluid flow between two co-axial tubes with peristalsis. Scientific Reports 13 (2023), 11013.
69. Ibrahim and M.Y. Abouzeid, Computational simulation for MHD peristaltic transport of Jeffrey fluid with density-dependent parameters. Scientific Reports 13 (2023), 9191.